Wideband and high-gain circularly-polarized L-shaped slot antenna array using metamaterial

Qiang Chen[1] (iD), Guolin Zhang[2], Changhui He[1], Ya Fan[1], Zhenbo Zhu[1], Di Zhang[1], Jing Li[1] and Yuanqing Zhao[3]

[1]Air Force Early Warning Academy, Wuhan, Hubei 430019, China; [2]School of Mathematical and Computer Science, Yichun University, Yichun, Jiangxi 336000, China and [3]The 93552 Troop of Chinese People's Liberation Army, Shijiazhuang, China

Abstract

This research involves a compact wideband circularly-polarized antenna array, which consists of a sequential rotating phase feed network, 2×2 mushroom-type metamaterial (MTM) unit, and so on. Each antenna array unit contains a microstrip feedline, an L-shaped slot antenna, and so on. The MTM-based antennas were incorporated with a sequential-phase network of sequentially rotated series-parallel feed to achieve wideband operation. The operational bandwidth and the radiation model in the high-frequency area were improved through the adjustment of spacing between the L-shaped slots while maintaining the size and structure of the MTM. The proposed design had dimensions of $80 \text{ mm} \times 80 \text{ mm} \times 3.5 \text{ mm}$ ($\sim 1.64 \lambda_0 \times 1.64 \lambda_0 \times 0.072 \lambda_0$ at 6.15 GHz), and it was simulated, fabricated, and tested.

Introduction

Circularly-polarized (CP) antennas receive a lot of attention due to their ability to combat polarization mismatch losses and multi-path interferences. A unique strategy for achieving circular polarization is introducing perturbation through corner truncation or etched slot [1]. CP microstrip antennas (MPAs) contain two core feed types, namely, dual or multi-feed type, and single-feed type. Although it has a portable structure, the single-feed CP MPAs have the disadvantages of narrow bandwidth and limited axial ratio (AR) bandwidth [2]. The narrow bandwidth of single-feed CP MPAs is solved through techniques such as the use of parasitic or stacked patches [3]. These solutions create the disadvantages of increased thickness or low radiation effectiveness. High-gain CP antenna arrays are used for improving the bandwidth of single-feed CP MPAs. However, this complicates their feeding network and multilayer structure.

A sequential-phase (SP) feed is used in developing operational bandwidth and antenna gain for patch antenna arrays [4]. The SP feed produces CP radiation with patch antennas that are polarized linearly [5]. SP feed has been employed in antenna array designs for various applications [6–10]. Such arrays use a truncated patch antenna as the original radiation factor; thus, <13% of operational bandwidths were insufficient for several applications. Two-by-two H-shaped patch antennas [6] have been incorporated into feeding networks based on a metamaterial (MTM) line for achieving wideband operation. At 2.5 GHz, the size of the entire array is $1.67 \lambda_0 \times 2.17 \lambda_0 \times 0.15 \lambda_0$, the gain bandwidth is 55.0%, and the AR bandwidth is 89.3%. Multilayer configurations and feeds, based on MTM lines and lumped factors, are rather complex. Using metasurfaces, the performance of antennas is improved to achieve mutual coupling reduction within the array, support the development of AR features, polarization conversion, antenna miniaturization, suppression of surface waves, gain enhancement, and the development of impedance matching [11, 12]. Recently, a global bandwidth of over 20% was reported for antenna arrays that rotate sequentially and use metasurfaces [13]. Such arrays have the disadvantage of high side lobe level (SLL). This paper proposes an MTM-based CP slot antenna array with low cost, broadband, portable size, and simple configuration. The proposal consists of a series of 2×2 CP L-shaped and MTM-based slot antennas incorporated with a series-parallel feed that rotates sequentially to achieve portable size and wideband operation [14, 15]. Corner-cutting patch antennas can achieve broadened bandwidth through the metasurface of a lattice of 4×4 periodic metal plates [16]. Owing to surface waves propagating on the metasurface, additional resonant frequencies are produced that make it possible to enhance bandwidths and improve gain. Some academic literary works, including [16], have suggested bandwidth enhancement and improvement can be achieved through loading the metasurface covering [16]. Bandwidth enhancement is limited to applying covering to various source antennas and metasurfaces. Owing to its wideband of reflection coefficients, slot antennas are widely applied in communication systems, GPS, and so on. This paper focused on incorporating MTM in a slot antenna and achieving satisfactory results despite traded-offs regarding
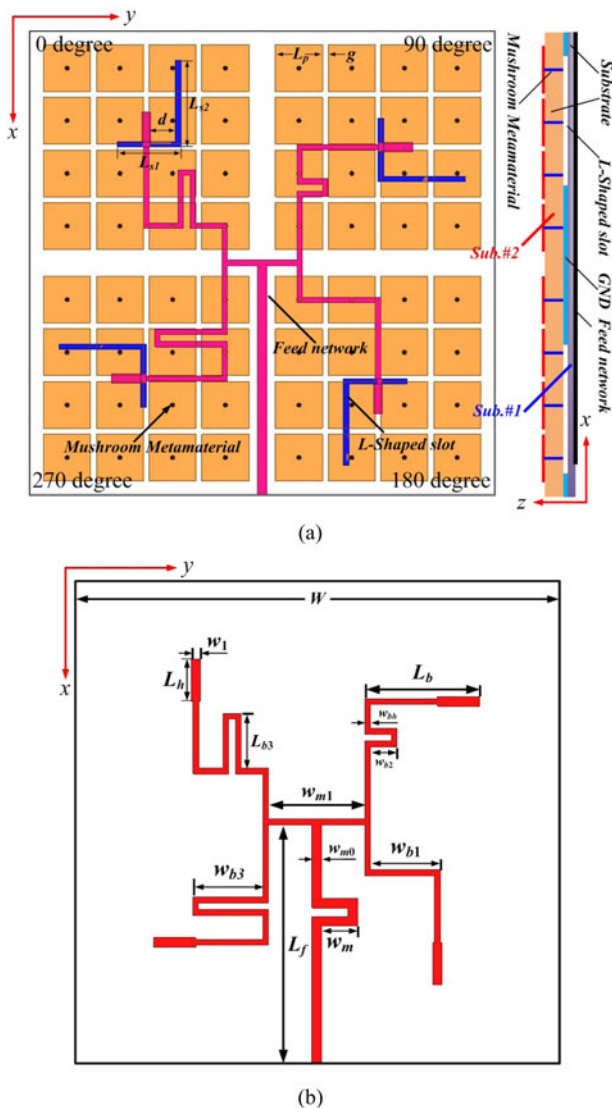
Fig. 1. Geometry of the CP MTM-based antenna array; (a) side and top views, and (b) geometry of feeding network.

Table 1. The optimal dimensions of the proposed antenna

Dimension	Size (mm)	Dimension	Size (mm)
L_{s1}	11	L_b	19
L_{s2}	15	w_{b3}	11.61
D	6	L_{b3}	9.11
L_p	8.1	L_h	7
G	1	w_1	1.5
L_f	27	w_{m1}	16
w_m	6	w_{bh}	0.89
w_{m0}	1.5	w_{b2}	4.41
w_{b1}	11.555		

gap in order to ease fabrication. The radiation mechanism and fundamental design of the single factor have some similarities with those of the antenna shown in [14]. In other words, it was made up of a ground plane etched with L-shaped slots, sandwiched between MTMs of a periodic structure with 4×4 metallic square plates, and short pins linking to the ground plane. Surface waves propagating through the metasurface were excited, creating other resonances and minimum AR points for broadening AR bandwidth and impedance. The optimal dimensions of the antenna were obtained through numerical simulation experiments, as listed in Table 1.

The L-shaped slot antenna, based on mushroom MTM, was fed by a microstrip line to ease integration with the SP network. The SP network was modified by a series-parallel strip with a curved structure, designed to equally distribute signals from the microstrip-line input to four microstrip-line outputs with phases of 270, 180, 90, and 0° [17]. Seven quarter-wavelength impedance transformers were connected in sequential rotation with a series of links and alternative parallel for achieving the required output phases and impedance matching. The SP network was designed for matching to a 50 Ω subminiature version A (SMA) connector. The center frequency was selected as 6.15 GHz. Four CP L-shaped slot antennas were arranged in sequential rotation and incorporated into the SP network to achieve wideband operation. Isolation and SLL factors were proportional to center-to-center spacing. A vertical part-to-center spacing of 7 mm ($\sim 0.6 \lambda_0$ at 6.5 GHz) was selected for the primary array to ensure sufficient isolation and low SLL. Due to the gradually increasing center-to-center spacing of the wavelength (32.6 mm is $0.71 \lambda_0$ at 6.5 GHz), the radiation model of the primary array degrades within the high-frequency area – particularly the SLL – relative to the center frequency. Spacing between the L-shaped slots d was decreased while maintaining metasurface size and structure for mitigating issues. Decreasing spacing between the L-shaped slots was limited by allowance for an SP network, so spacing between L-shaped slots $d = 6.0$ mm ($\sim 0.5 \lambda_0$ at 6.5 GHz). The L-shaped slots had an off-center position, related to MTM in terms of the ultimate array's single factor. The antenna was designed on ANSYS HFSS to achieve 3 dB AR bandwidths, wide impedance matching, low profile, high gain with low variation, and a radiation model with low SLL. The optimized design parameters of the antenna are shown in Table 1.
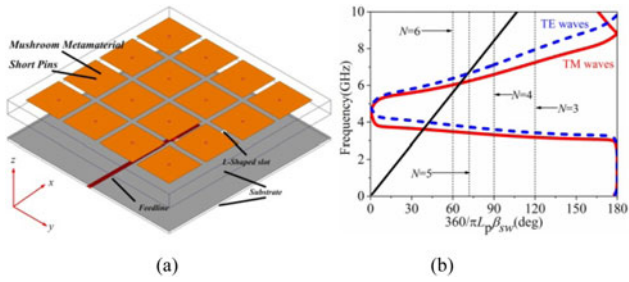
dimensions. For the purpose of developing a radiation model in the high-frequency area, the spacing among L-shaped slots was appropriately adjusted while maintaining metasurface size and structure. The proposed design was validated via experiments using the ANSYS high-frequency structure simulator (HFSS).

Antenna configuration and analysis

Geometry of the antenna array

Figure 1 presents the geometry of the proposed antenna array, made up of a series of 2×2 mushroom L-shaped and MTM-based slot antennas, powered by an SP network. The substrates consist of Duriod material (tanδ = 0.0027, ε_r = 2.65) and F4B (tanδ = 0.0009, ε_r = 2.2) with thicknesses h_2 = 3.0 mm and h_1 = 0.5 mm, respectively. The SP network was printed on the bottom and top sides of substrate #1 and substrate #2, respectively. The L-shaped slots were etched on the ground plane, while the mushroom MTM structures were put on substrate #2 as the radiation part. Substrate #2 was stacked over substrate #1 without air

Fig. 2. (a) Geometry of the single factor, (b) dispersion diagram of the graphical solution, and the MTM structure of equation (1) for different numbers of unit cells.
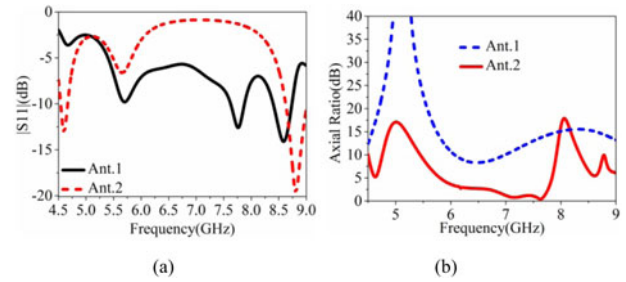

Fig. 4. AR and simulated reflection coefficients of various antenna designs; (a) S11 and (b) AR.
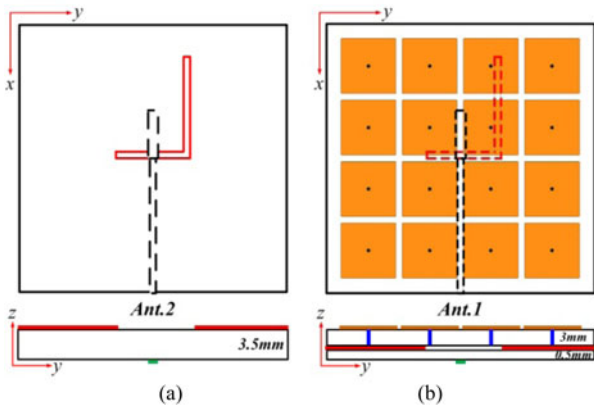

Fig. 3. Various configurations of microstrip-fed L-shaped slot antennas; (a) without MTM superstrate and (b) with MTM superstrate.

Fig. 5. Configuration of the metasurface-based L-shaped slot antenna array.

Analysis of the single-element design

The single factor's geometry is described in Fig. 2(a), and the MTM structure's dispersion was calculated within the connected boundary conditions using HFSS software [18]. The original eigenmodes were calculated and shown in Fig. 2(b). The surface wave resonance point is mainly obtained using graphical methods, and it was obtained as the intersection of the dispersion curve and equation (1). When $N = 3$, transverse magnetic (TM) and transverse electric (TE) waves are 7.25 and 7.95 GHz, respectively; when $N = 4$, 6.6, and 7.12 GHz, respectively; when $N = 5$, 6.23, and 6.66 GHz, respectively; and when $N = 6$, 6.03, and 6.38 GHz, respectively. Referring to Fig. 3, the bandwidth properties of L-shaped slot antennas with and without MTM superstrates are compared to verify the superiority of the proposed design. Referring to Fig. 4(a) and 4(b), the L-shaped slot antenna yielded one minimum point with the AR profile and three resonances with the |S11| profile. Thus, the existence of surface-wave resonances in the proposed antenna can be verified through the introduction of minimum points and extra resonances within the AR and SLL profiles, respectively.

Fig. 6. Simulated outcomes for various kinds of L-shaped slot antennas with MTM superstrate and with MS superstrate: (a) |S11| and (b) AR and broadside gain.
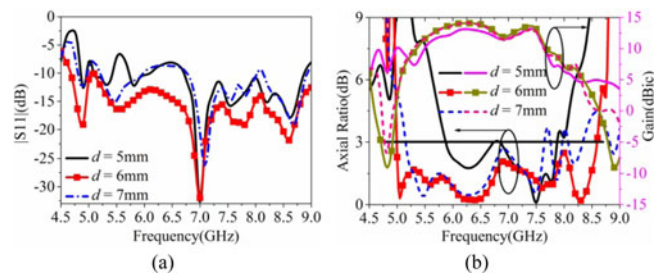
Fig. 7. Simulated outcomes of the suggested array antenna for different distances between the L-shaped slots: (a) |S11| and (b) AR and gain.

$$\beta_{SW} = \frac{\pi}{L_g}, \qquad (1)$$

where β_{SW} is the propagation constant of the wave resonances, which has been discussed above, and L_g is the overall length of the metasurface structure, given by equation (2).
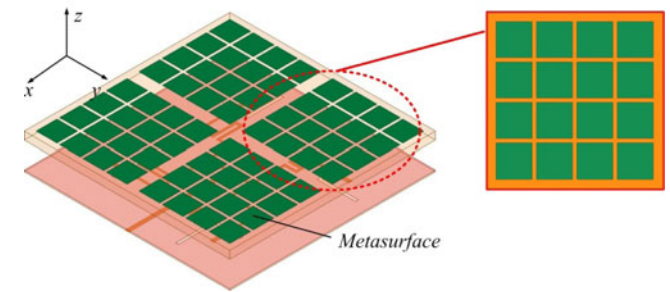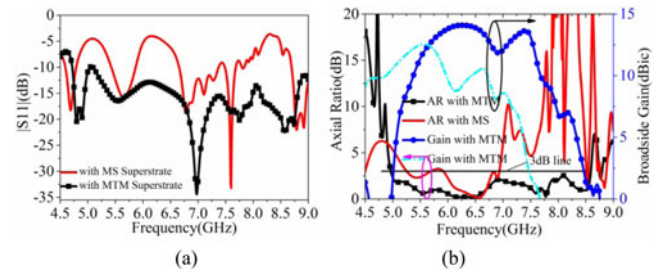
$$L_g = N \times L_p, \qquad (2)$$

where P is the periodicity of the metasurface, and N is the number of unit cells.

The antenna units were arranged in a "chessboard" configuration. The antenna arrangement at various sections avoided

Fig. 8. Fabrication of the proposed antenna array.

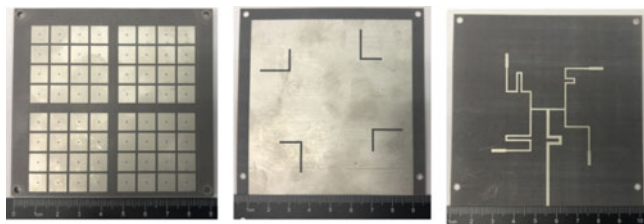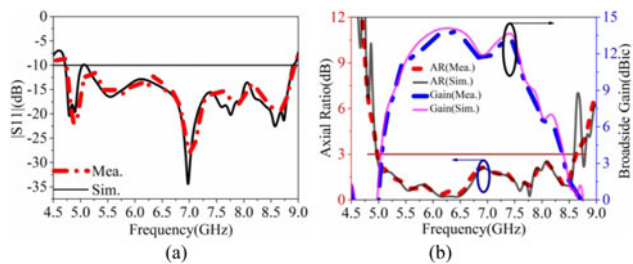**Fig. 9.** Real-world and simulation results: (a) |S11| and (b) axial ratio and broadside gain.

in-phase exciting to prevent model troughs in the composite radiation fields [18]. A sequentially rotated feeding network was necessary for the antenna array to realize sufficient CP radiation features. Figure 1(a) shows the fending phase of the units and the schematic diagram of the antenna array. The LP and CP units were able to achieve the desired radiation features. The overall gain of the antenna array was relative to the unit's polarization state.

Referring to Fig. 2, it was necessary to use right-hand circularly-polarized (RHCP) units in order to realize the desired circular polarization radiation feature. The overall *E*-field left-hand circularly-polarized radiation is calculated using equation (3).

$$\vec{E}_t^{RHCP} = \frac{\sqrt{2}}{2}\vec{E}_0[(\vec{y}+j\vec{x})e^{j0°} + (\vec{x}-j\vec{y})e^{j90°} + (-\vec{y}-j\vec{x})e^{j180°}$$
$$+ (-\vec{x}+j\vec{y})e^{j270°}] = \frac{\sqrt{2}}{2}E_0(4\vec{y}+j4\vec{x}) = 2\sqrt{2}E_0(\vec{y}+j\vec{x}).$$
$$(3)$$

It is shown in Fig. 3 that the MTM-based configuration yielded a narrow bandwidth when functioning with low gain and AR and |S11| profiles. Nevertheless, the co-polarization's broadside gain, impedance matching, and CP bandwidths increase significantly because of the mushroom cells' loading instead of covering by the MS array as displayed in Fig. 5.

According to Fig. 6, the metasurface-based configuration yielded a narrow bandwidth when functioning with low gain and AR and |S11| profiles. However, broadside gain, impedance matching, and CP bandwidths increase significantly due to the metamaterial superstrate.

As discussed earlier, the array's radiation model within the high-frequency area is influenced by changing the spacing between the L-shaped slots while maintaining the entire size and structure of the MTM. To demonstrate this, the proposed design is simulated with different spacing values *d*, and the results are presented in Fig. 7(a) and 7(b). Appropriately
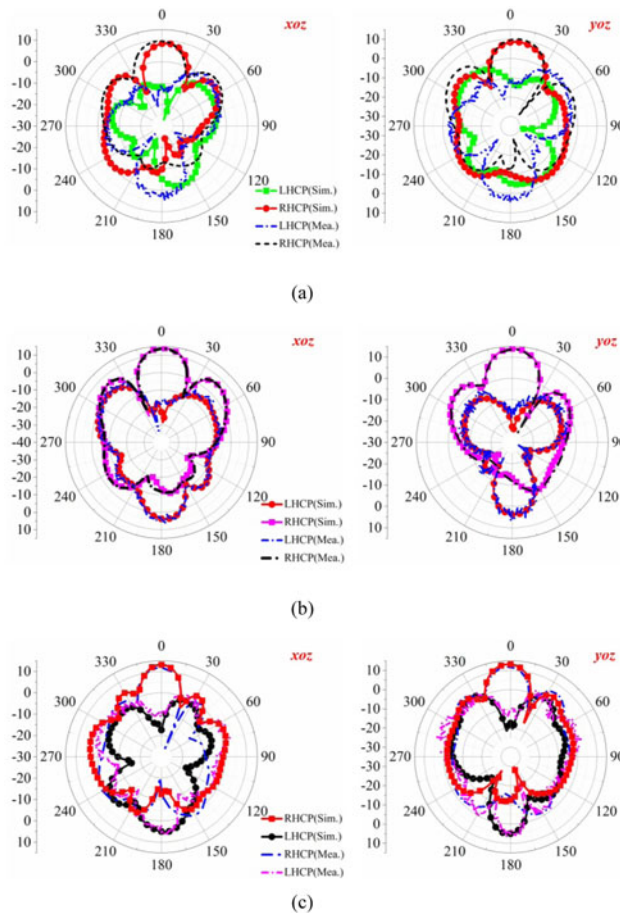

Fig. 10. Simulation and real-world radiation models of the proposed array at (a) 5.5 GHz, (b) 6.5 GHz, and (c) 7.3 GHz.

adjusting *d* significantly increased the array's bandwidth and improved the radiation model within the high-frequency area. According to Fig. 7, *d* = 6 mm created a |S11| bandwidth, wider AR, and lower SLL in comparison to *d* = 7 mm and *d* = 5 mm.

Real-world and simulation results

For the purpose of verification, the proposed design was simulated, fabricated, and tested. A sample fabrication prototype is shown in Fig. 7(a). In comparison with the simulation model, substrate #1 of the fabrication prototype was extended by 10 mm for the purpose of fastening a 3.5 mm SMA connector. The size of the fabricated array was 90 mm × 80 mm × 3.5 mm, as shown in Fig. 8.

Figure 9(a) presents the *S*-parameters of the proposed antenna, obtained from simulation and real-world testing. The simulated S11 was below −10 dB for 4.6–8.8 GHz. The simulated isolation was below 15 dB at most impedance bandwidths. According to real-world measurements, the antenna may possess an impedance bandwidth of 62.7% (4.6–8.8 GHz) for S11 < −10 dB. The simulation and real-world outcomes were in line with expectations. The measured ARs and gain versus frequency plot are presented within Fig. 9(b). Referring to Fig. 9(b), the 3 dB AR bandwidth measured from simulation and real-world testing could both be 56.7% (4.8–8.6 GHz). The real-world measurements slightly

Table 2. Performance comparison of the proposed design and other MTM-based antenna arrays

Antenna structure	Dielectric constant (upper/lower)	Overall antenna volume (λ_0^3) or miniaturization electrical size	−10 dB |S11| BW (%)	3 dB AR BW (%)	3 dB Gain BW (%)	Peak gain (dBic)
Proposed	2.65/2.2	1.64 × 1.64 × 0.072	62.7	56.7	37.3	14.10
[16]	3.38/3.38	1.26 × 1.26 × 0.046	55.6	41.67	37.3	12.08
[19]	4.2/4.2	1.72 × 1.72 × 0.077	75.4	46.5	24.4	12.80
[13]	3.38/3.38	1.60 × 1.60 × 0.065	41.45	23.16	22.68	13.5
[6]	3.38/3.55	1.67 × 2.17 × 0.150	85.4	89.3	55.0	11.0
[8]	2.4/4.4	1.67 × 1.67 × 0.058	6.0	5.8	5.21	10.5
[14]	2.2/2.2	1.36 × 1.36 × 0.08	48.2	35.5	35.8	10.9
[20]	2.65/9.8	Not given	More than 20%	20	Not given	15
[21]	2.2/6.15	Not given	24.6	21	19.7	20

BW, bandwidth.

deviate from those predicted by HFSS simulation. This deviation can be attributed to the tolerance of the fabricated antenna array.

Figure 10 presents the simulated and real-world radiation models at 7.3, 6.5, and 5.5 GHz in the *yoz* and *xoz* planes, respectively. The proposed L-shaped slot MTM-based antenna possesses steady radiation models within the operating bandwidth. At 5.5 GHz, the measurements show an SLL of <−20 dB and a front-to-back ratio of 21 dB, and the HPBW corresponding to the *xoz* and *yoz* planes was 31 and 38°, respectively. At 6.5 GHz, the measurements show that the corresponding *xoz* and *yoz* planes are 34 and 32°, respectively, when SLL does not exceed −18 dB. At 7.3 GHz, the measurements show that when the front-to-back ratio is 25 dB, SLL does not exceed −14 dB, and the corresponding *xoz* and *yoz* planes were 30 and 29°, respectively. The proposed design was compared with other MTM-based antennas, as presented in Table 2. The proposed design has a portable size, the broadest 3 dB AR bandwidth, and the broadest impedance bandwidth.

Conclusions

The paper described a portable wideband CP antenna array, employing a mushroom-like MTM. The antenna array consists of a series of 2 × 2 CP L-shaped and MTM-based slot antennas, incorporated with an SP network for the purpose of achieving wideband operation. The antenna array caused a steady LHCP radiation with a 3 dB gain and a bandwidth of 4.8–7.0 GHz (37.3% and peak gain of 14.1 dB). The proposed antenna array is a viable candidate for wideband wireless communication systems, because of its simple configuration, steady radiation profile, wide operating frequency, low profile, and high gain.

References

1. **Nasimuddin, Chen ZN and Qing X** (2012) Compact circularly polarized asymmetric-slotted microstrip patch antennas. *Microwave & Optical Technology Letters* 54, 1920–1927.
2. **Wang Z, Fang S, Fu S and Jia S** (2011) Single-fed broadband circularly polarized stacked patch antenna with horizontally meandered strip for universal UHF RFID applications. *IEEE Transactions on Microwave Theory and Techniques* 59, 1066–1073.
3. **Ding K, Gao C, Yu T, Qu D and Zhang B** (2016) Gain-improved broadband circularly polarized antenna array with parasitic patches. *IEEE Antennas & Wireless Propagation Letters* 2017, 1468–1471.
4. **Huang J** (1995) A Ka-band circularly polarized high-gain microstrip antenna array. *IEEE Transactions on Antennas and Propagation* 43, 113–116.
5. **Huang J** (1986) A technique for an array to generate circular polarization with linearly polarized elements. *IEEE Transactions on Antennas and Propagation* AP-34, 1113–1124.
6. **Chung K** (2013) High-performance circularly polarized antenna array using metamaterial-line based feed network. *IEEE Transactions on Antennas and Propagation* 61, 6233–6237.
7. **Yang W, Zhou J, Yu Z and Li L** (2014) Bandwidth and gain enhance circularly polarized antenna array using sequential phase feed. *IEEE Antennas Wireless Propagation Letters* 13, 1215–1218.
8. **Li Y, Zhang Z and Feng Z** (2013) A sequential-phase feed using a circularly polarized shorted loop structure. *IEEE Transactions on Antennas and Propagation* 61, 1443–1447.
9. **Deng C, Li Y, Zhang Z and Feng Z** (2014) A wideband sequential-phase fed circularly polarized patch array. *IEEE Transactions on Antennas and Propagation* 62, 3890–3893.
10. **Chen A, Yang Y, Chen Z and Cao S** (2010) A Ka-band high-gain circularly polarized microstrip antenna array. *IEEE Transactions on Antennas and Propagation* 9, 1115–1118.
11. **Dong Y and Itoh T** (2012) Metamaterial-based antennas. *Proceedings of the IEEE* 100, 2271–2285.
12. **Holloway CL, Kuester EF, Gordon JA, O'Hara J, Booth J and Smith DR** (2012) An overview of the theory and applications of metasurfaces: the two-dimensional equivalents of metamaterials. *IEEE Antennas and Propagation Magazine* 54, 10–35.
13. **Ta SX and Park I** (2016) Planar, high-gain, wideband, circularly polarized metasurface-based antenna array. *Journal of Electromagnetic Waves and Applications* 30, 1620–1630.
14. **Chen Q, Zhang H, Shao YJ and Zhong T** (2018) Bandwidth and gain improvement of an L-shaped slot antenna with metamaterial loading. *IEEE Antennas Wireless Propagation Letters* 17, 1411–1415.
15. **Zhang WB, Liu Y and Jia Y** (2018) Circularly polarized antenna array with low RCS using metasurface-inspired antenna units. *IEEE Antennas Wireless Propagation Letters* 18, 1453–1457.
16. **Ta SX and Park I** (2017) Compact wideband circularly polarized patch antenna array using metasurface. *IEEE Transactions on Antennas and Propagation* 16, 1932–1936.
17. **Chung K, Chaimool S and Zhang C** (2015) Wideband subwavelength-profile circularly polarised array antenna using anisotropic metasurface. *Electronics Letters* 51, 1403–1405.
18. **Jia Y, Liu Y, Zhang W, Wang J and Liao G** (2018) In-band radar cross section reduction of slot array antenna. *IEEE Access* 6, 23561–23567.

19. **Chung K, Chaimool S and Zhang C** (2015) Wideband subwavelength-profile circularly polarised array antenna using anisotropic metasurface. *Electronics Letters* **51**, 1403–1405.

20. **Zarbakhsh S, Akbari M, Farahani M, Ghayekhloo A, Denidni TA and Sebak A** (2020) Optically transparent subarray antenna based on solar panel for CubeSat application. *IEEE Transactions on Antennas and Propagation* **68**, 319–328.

21. **Zarbakhsh S, Akbari M, Samadi F and Sebak A** (2019) Broadband and high-gain circularly-polarized antenna with low RCS. *IEEE Transactions on Antennas and Propagation* **67**, 16–23.

Qiang Chen was born in Jiangxi, China. He received the master and Ph.D. degree from Air Force Engineering University (AFEU), Xi'an, China, in 2015 and 2019, respectively. He is currently a lecturer of Air Force Early Warning Academy, Wuhan, Hubei, China. His research interests include microwave circuits, antennas, and arrays.

Guolin Zhang was born in Jiangxi, China. He received the bachelor degree from Shenyang University of Technology, Shenyang, China, in 1991. His research interests include computer communication and network technology.

Changhui He was born in 1973. She received the master degree from Central China Normal University. She is currently an associate professor of Air force early warning institute. She is interested in electromagnetic field, microwave technology, and antenna design. She has published over 20 technical papers and authored one book. She is holding four national invention patents.
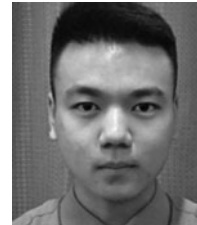
Ya Fan received the B.S. degree from Air Force Engineering University, Xi'an, China, 2013; the M.S. degree in physical electronics from Air Force Engineering University, Xi'an, China, 2015; the Ph.D. degree in physical electronic from Air Force Engineering University, Xi'an, China. From 2015 to the present, he has been employed in Air Force Early Warning Academy, where he is currently a lecturer of the department of information countermeasure. His research interests are mainly on surface plasma polaritons, design and applications of metasurfaces, metasurface-inspired antenna, and microwave devices.

Zhenbo Zhu was born in Wuhan, China, in 1977. He received the M.S. degree from Air Force Early Warning Academy, Wuhan, China, in 2003. He received the Ph.D. degree in electrical engineering from Navy Engineering University, Wuhan, China, in 2007. He is currently an associate professor of the Air Force Early Warning Academy. His current research interests include radar target detection and imaging.

Di Zhang received the B.S., M.S., and the Ph.D. degrees from Air Force Engineering University (AFEU), Xi'an, China, in 2013, 2015, and 2019, respectively. He is currently a lecturer with Air Force Early Warning Academy. His research interests include RF orbital angular momentum antennas, reflect array antennas, and metasurface.

Jing Li received the Ph.D. degree in information and communication engineering from Huazhong University of Science and Technology, Wuhan, China, in 2013. He is currently a lecturer of Air Force Early Warning Academy. His research interests include optical communication systems, EW antennas, and signal processing.

Yuanqing Zhao was born in 1989. She received the master degree from Air Force Engineering University. She is interested in signal and information processing. Now she is mainly working on the research of communication and navigation technology.